Pictorial Essay | Pediatric Imaging

eISSN 2005-8330
https://doi.org/10.3348/kjr.2019.0500
Korean J Radiol 2020;21(2):146-158

Korean Journal of Radiology
KJR

Ultrasonographic Demonstration of the Tissue Microvasculature in Children: Microvascular Ultrasonography Versus Conventional Color Doppler Ultrasonography

Joonghyun Yoo, MD[1], Bo-Kyung Je, MD, PhD[1], Ji Yung Choo, MD, PhD[2]

[1]Department of Radiology, Korea University Hospital, Ansan, Korea; [2]K Eye Clinic, Hongseong, Korea

Microvascular ultrasonographic imaging is the most recent and unique Doppler ultrasound technique. It uses an advanced clutter filter that can remove clutter artifacts and preserve the low-velocity microvascular flow signal. The potential advantages of microvascular ultrasonography are its superiority in detection and visualization of the small blood vessels in tissues, providing radiologists with more information on the vascular structures. Therefore, it has shown particular value in the clinical fields. The aim of this study was to provide microvascular ultrasonographic images for the tissue microvasculature, including the brain, thyroid gland, kidney, urinary bladder, small bowel, ovary, testis, lymph node, and hemangiomas in children, focusing on the comparison with conventional color Doppler ultrasonographic images.

Keywords: *Children; Ultrasonography; Blood vessels; Microvascular imaging; Ultrasonography, doppler, color*

INTRODUCTION

Ultrasonography (US) is the most common imaging modality used for children. Microvascular US (MVUS) uses an innovative Doppler ultrasound algorithm and has an improved diagnostic ability. Conventional color Doppler US (CDUS) uses wall filters, which apply the appropriate cutoff frequency to suppress the low-frequency components resulting from patients' motion, pulsation, and respiration, called clutter artifacts (Fig. 1A). When clutter artifacts are eliminated from the acquired signals, true low-velocity blood flow is also eliminated because of overlapping frequency. Power Doppler US (PDUS) is a second-generation Doppler technique that shows the strength of the acquired Doppler signal in color, regardless of the speed or direction of the moving cells. The number of moving cells is directly proportional to the intensity of paleness in the expressed color (1). PDUS is approximately three times more sensitive than CDUS; therefore, more small vessels can be visualized on grayscale US.

MVUS is a third-generation Doppler technique that was developed to overcome the limitations of conventional wall filters used in the preceding Doppler techniques that eliminate both clutter artifacts and slow blood flow. MVUS uses an advanced filter that can differentiate tissue artifacts from low-velocity blood flow by exploiting the spatiotemporal coherence information (Fig. 1B). This advanced filter can suppress the tissue component selectively and preserve the microvascular flow signal, which is otherwise filtered and removed in conventional CDUS (2). Since the first MVUS technique Superb Microvascular Imaging (SMI) was launched by Canon Medical Systems, other vendors have mounted MVUS filters on high-end US

Received July 5, 2019; accepted after revision September 25, 2019.
This study was supported by the Korea University College of Medicine (K1710761) and the Department of Radiology, Korea University College of Medicine.
Corresponding author: Bo-Kyung Je, MD, PhD, Department of Radiology, Korea University Hospital, 123 Jeokgeum-ro, Danwon-gu, Ansan 15355, Korea.
• Tel: (8231) 412-5229 • Fax: (8231) 412-5224
• E-mail: radje@korea.ac.kr

Korean Journal of Radiology
KJR

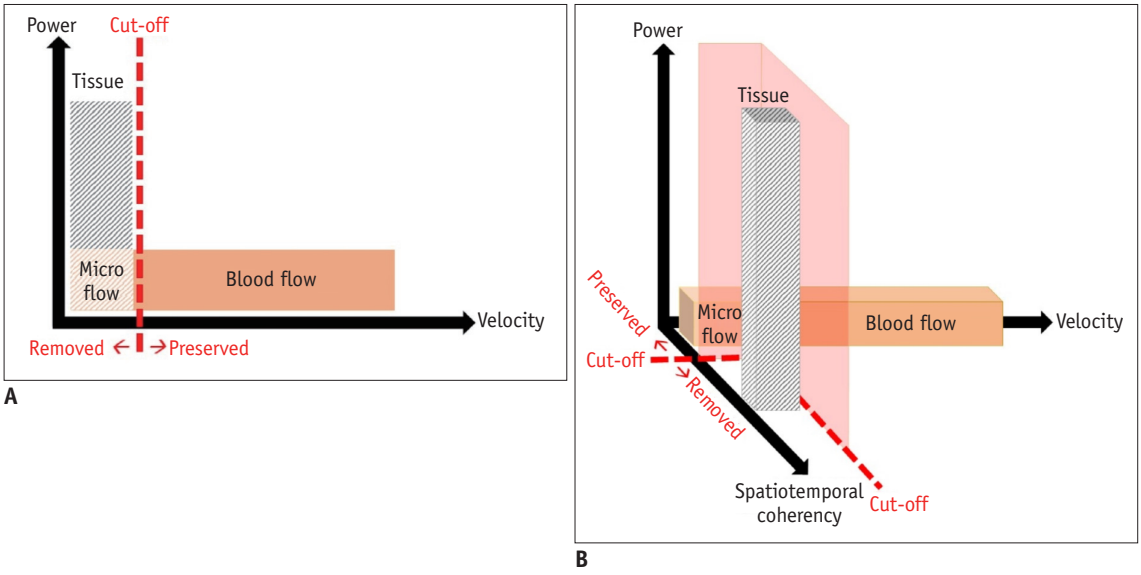

Fig. 1. Comparison of conventional clutter filter of color Doppler ultrasonography and advanced clutter filter of microvascular ultrasonography.
A. Conventional clutter filter of color Doppler ultrasonography cannot distinguish between tissues and low-velocity vessels using velocity information. **B.** Advanced clutter filter of microvascular ultrasonography makes it possible to extract low-velocity vessels by exploiting spatiotemporal coherence information.

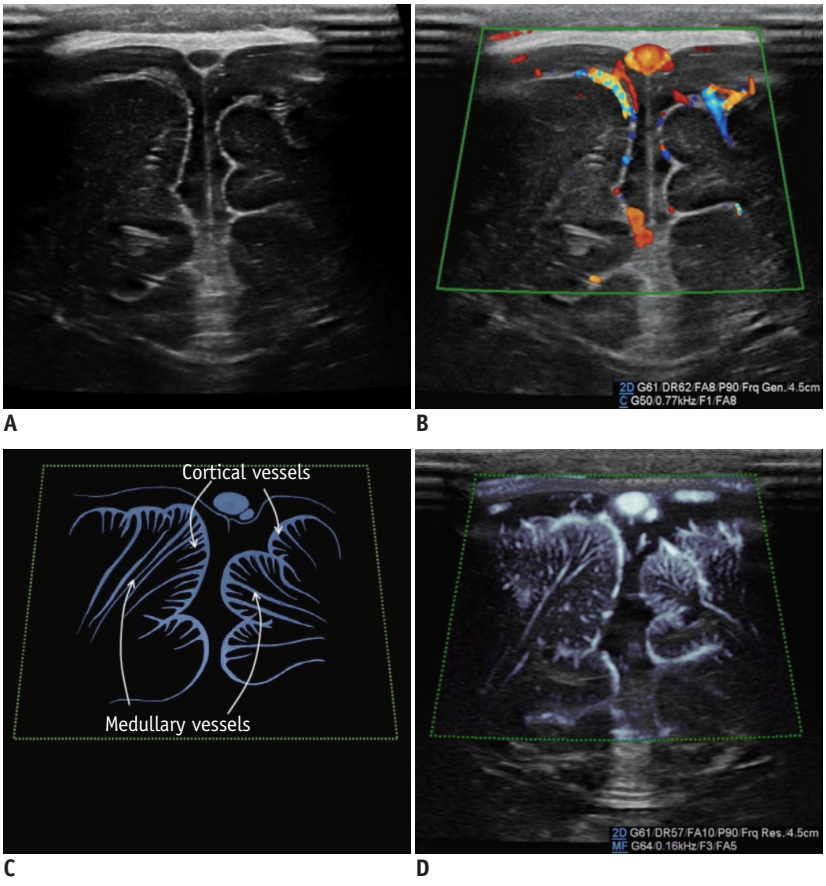

Fig. 2. Normal brain ultrasonography in 2-month-old boy.
A. Grayscale ultrasonography. **B.** Color Doppler ultrasonography shows leptomeningeal vessels covering gyri. **C.** Illustration indicates intracortical, subcortical, and medullary vessels, as seen on microvascular ultrasonography **(D)**. Parameters on Doppler images: DR = dynamic range, F = filter, FA = frame average, G = gain, P = power

https://doi.org/10.3348/kjr.2019.0500

devices to yield high-resolution MVUS images. In addition to previous studies using SMI in the pediatric population (3-7), we performed MVUS in children, using the MV-Flow™ of RS85, manufactured by Samsung Medison (Seoul, Korea). To compare the two Doppler techniques with the highest objectivity, the images were obtained while maintaining the initial parameters without the examiner's manipulation. MVUS allows visualization of both normal and pathologic microvascular tissue structures. The purpose of this pictorial essay was to review the MVUS images of normal perfusion patterns and different abnormal perfusion patterns of various tissues in children and to compare them with CDUS images.

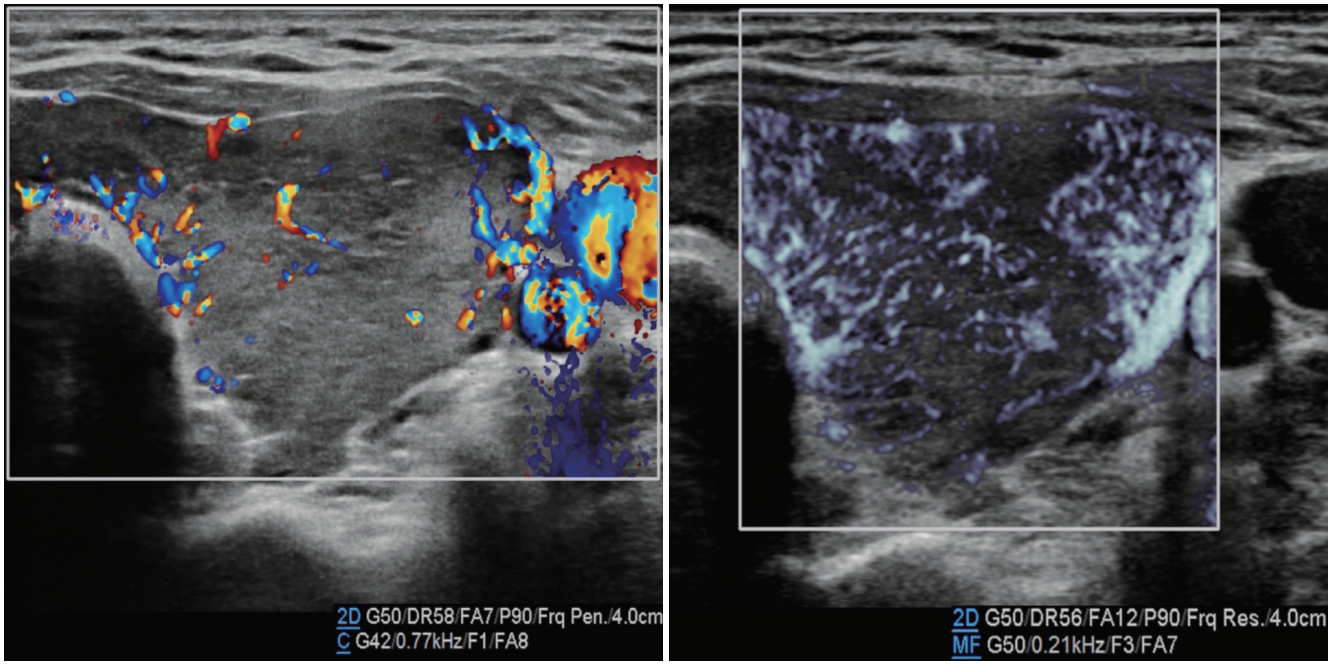

A B

Fig. 3. Thyroid ultrasonography in 14-year-old girl with toxic Grave's disease.
Microvascular ultrasonography image **(B)** shows status of vascularity better compared to color Doppler ultrasonography image **(A)**.

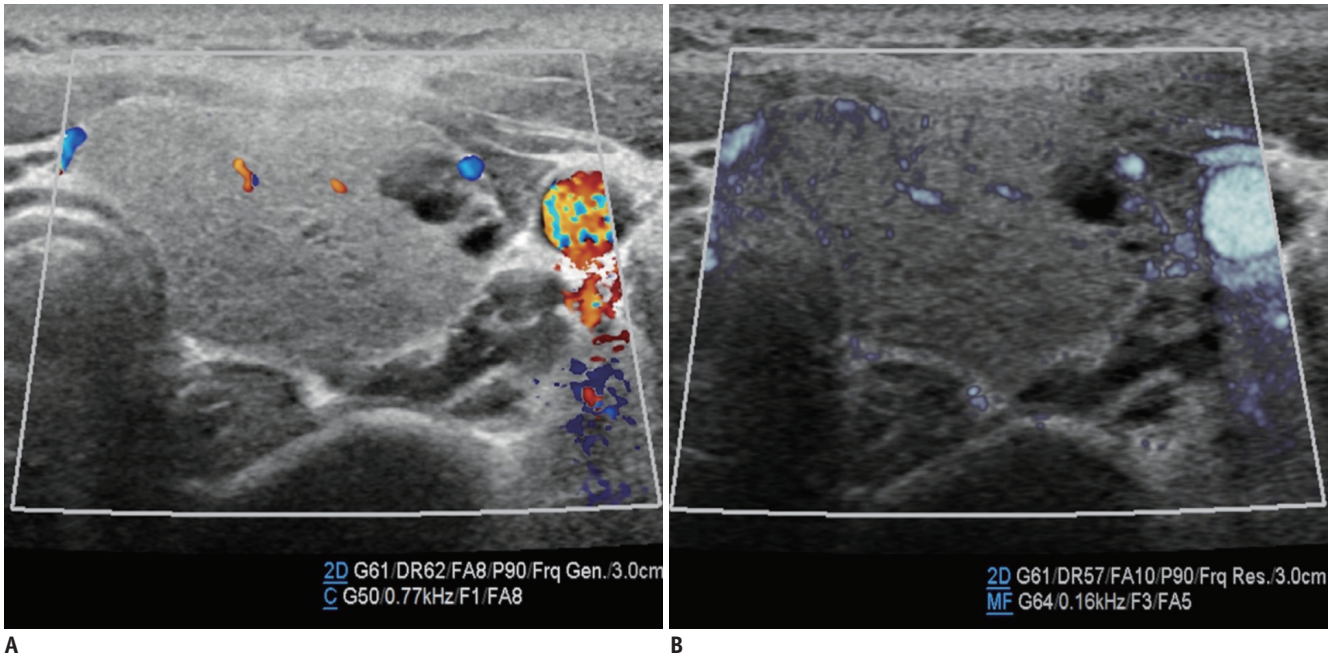

A B

Fig. 4. Thyroid ultrasonography in 13-year-old girl with non-toxic simple goiter.
Both color Doppler ultrasonography **(A)** and microvascular ultrasonography images **(B)** show scanty parenchymal vascularity of thyroid gland, which correlated with normal results of thyroid function tests (not shown here).

https://doi.org/10.3348/kjr.2019.0500

Korean Journal of Radiology
KJR

Brain

For neonates, transfontanelle brain US is the primary brain imaging modality because it provides easy accessibility, patient safety, and high-resolution images. Doppler studies can increase the clinical value of brain US performed for the vascular structures. The intracortical vessels arising from the pial arteries pass the cortex and branch into the following six groups depending on their degree of extension within the cortex: group 1 reaches the cortical layer; groups 2–4 pass through the entire cortical thickness; group 5 reaches the subcortical white matter; and group 6 (medullary artery) reaches the white matter (8). With conventional CDUS, the leptomeningeal vessels are seen on the superficial scans while the lenticulostriate perforators supplying the caudate and lentiform nuclei are seen on the deep scans (Fig. 2). On the MVUS images, we could define groups 1–5 as intracortical vessels and group 6 as medullary vessels supplying the cortex and white matter, respectively. Similarly, Goeral et al. (3) reported that SMI could distinguish between the striatal and extrastriatal vessels in their prospective study. The application of MVUS for pathologic condition in the pediatric brain has not been reported and should be further studied in the future.

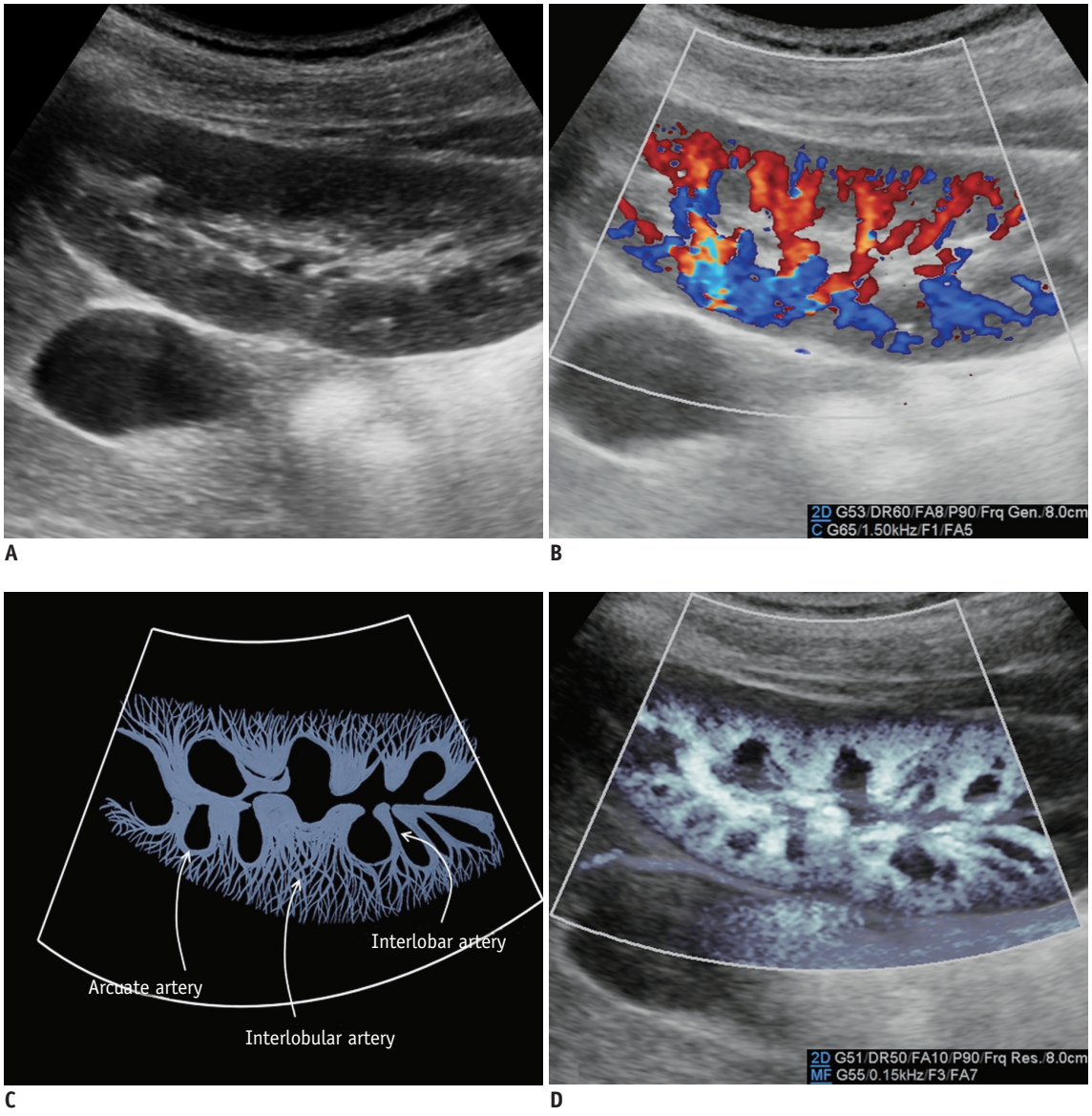

Fig. 5. Normal kidney ultrasonography in 10-year-old girl.
A. Grayscale ultrasonography. **B.** Color Doppler ultrasonography shows interlobar arteries and some arcuate and interlobular arteries. **C.** Illustration indicates interlobar, arcuate, and peripheral interlobular arteries filling renal cortex tightly, as seen on microvascular ultrasonography **(D)**. Microvascular ultrasonography also defines hypoechoic renal medulla clearly.

https://doi.org/10.3348/kjr.2019.0500

Thyroid Gland

US is the primary imaging modality used for evaluating the thyroid gland. Moreover, information on vascularity within the thyroid nodules can help diagnose malignancy associated with the thyroid nodules, in addition to the known characteristics, such as hypoechogenicity, irregular margins, "taller-than-wide" shape, and microcalcifications (9). MVUS might provide more detailed information on the microvascular architecture and vascular branching and distribution, thereby improving the diagnostic performance of the Thyroid Imaging Reporting and Data System for TR 4 thyroid nodules (10, 11). However, despite better depiction of the microvasculature, SMI has shown little benefit in the differential diagnosis of malignant and benign thyroid nodules (9).

We used MVUS for the thyroid parenchyma and to differentiate between normal and pathologic glands based on the vascularity and found that changes in the vascularity in thyroiditis and hyperthyroidism were more prominent on MVUS than on CDUS (Figs. 3, 4). In patients with thyroid goiter, the vascularity seemed to differ based on the thyroid function of the patients: It was more prominently increased in patients with toxic goiter than in those with non-toxic goiters. Although we could not apply the quantification

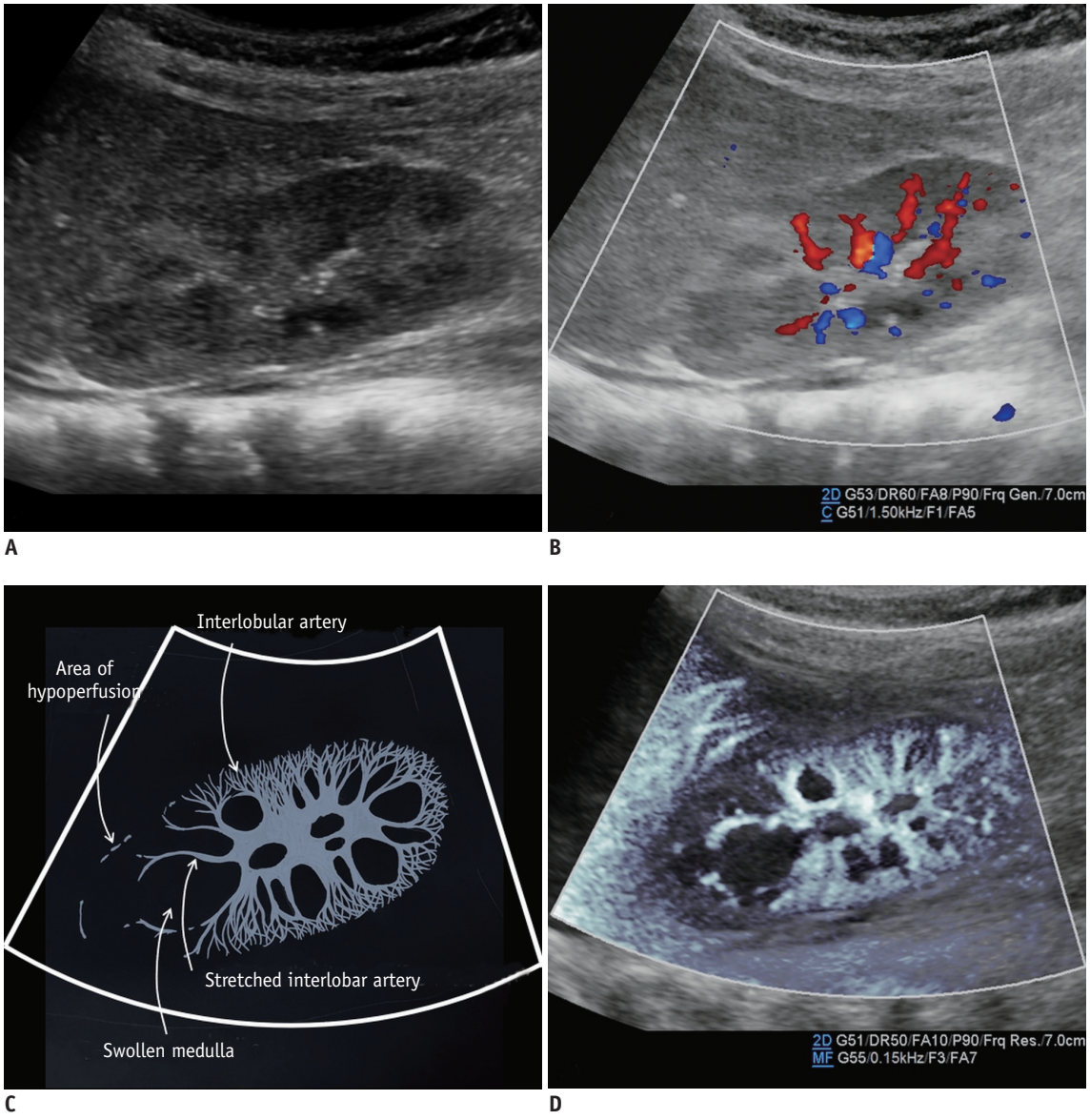

Fig. 6. Kidney ultrasonography in 5-month-old girl with acute pyelonephritis.
A. On grayscale ultrasonography, wedge-shaped, hyperechoic lesion is suspected at upper pole. **B.** Color Doppler ultrasonography shows area of hypoperfusion at upper pole. **C.** Illustration indicates area of hypoperfusion, interlobular arteries stretched by swollen medulla, and scanty interlobular arteries, as seen on microvascular ultrasonography **(D)**.

https://doi.org/10.3348/kjr.2019.0500

Korean Journal of Radiology
KJR

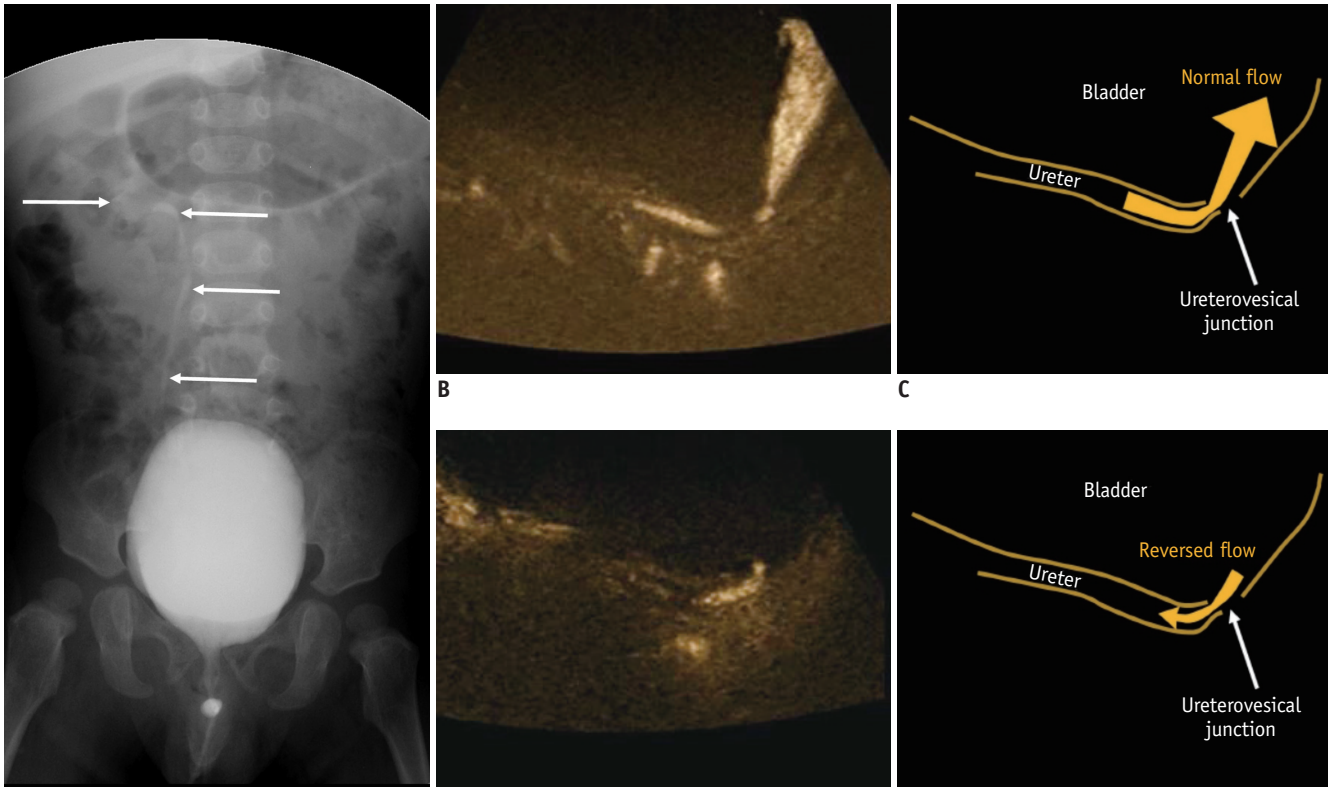

Fig. 7. Microvascular ultrasonography video clips and illustrations of 22-month-old boy with grade 2 vesicoureteral reflux confirmed on voiding cystourethrography.
A. Refluxed contrast media from urinary bladder in right ureter, renal pelvis, and calyces without dilatation (arrows). **B, C.** Normal urine flow from distal ureter to urinary bladder (**B;** Supplementary Movie 1). **D, E.** Reversed urine flow from ureterovesical junction to distal ureter (**D;** Supplementary Movie 2).

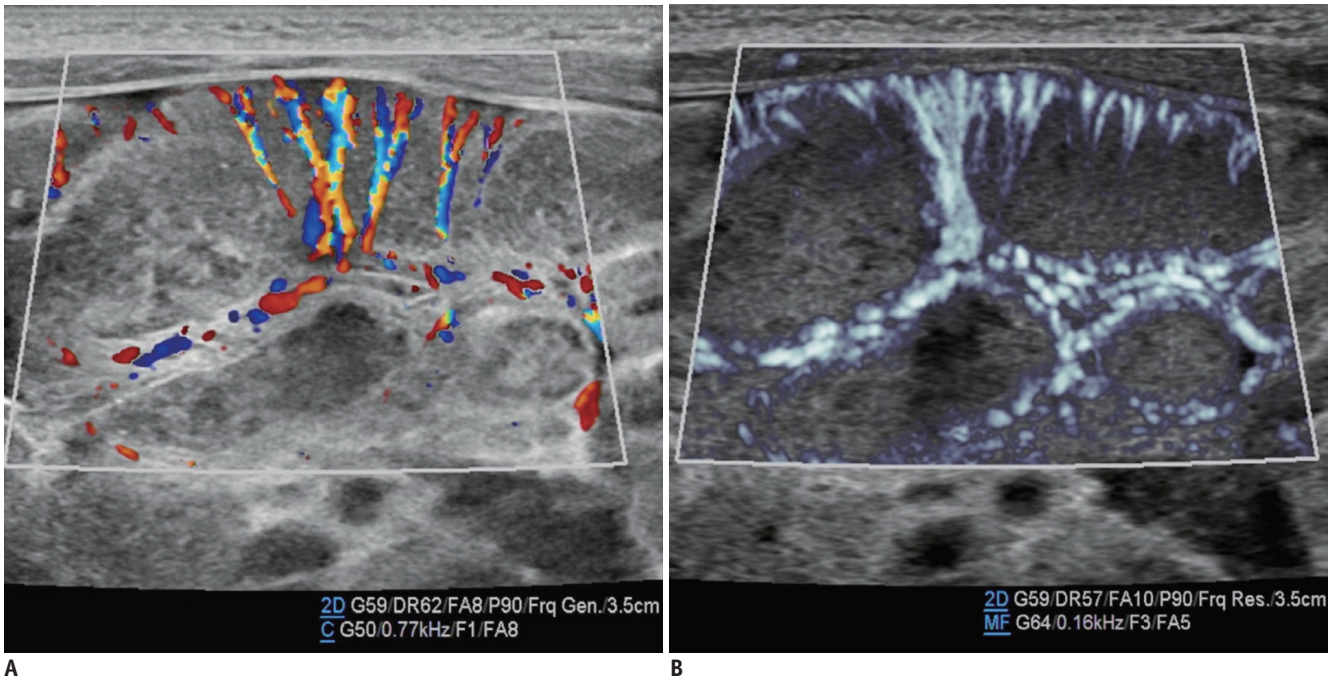

Fig. 8. Small bowel ultrasonography in 3-day-old boy with adenoviral enteritis.
Microvascular ultrasonography image **(B)** shows vasa recta and vessels circumscribing bowel wall better compared to color Doppler ultrasonography image **(A)**.

https://doi.org/10.3348/kjr.2019.0500

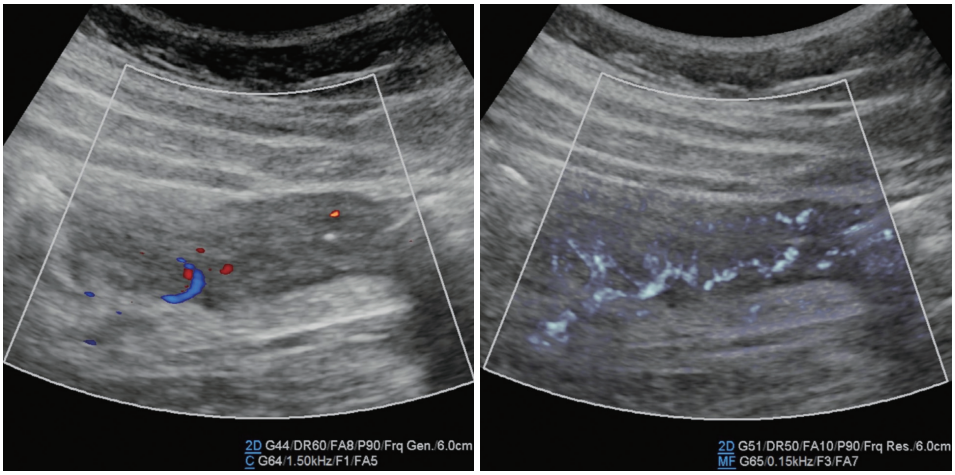

Fig. 9. Small bowel ultrasonography in 16-year-old girl with tuberculous enteritis.
Microvascular ultrasonography image **(B)** shows transmural vessels better compared to color Doppler ultrasonography image **(A)**.

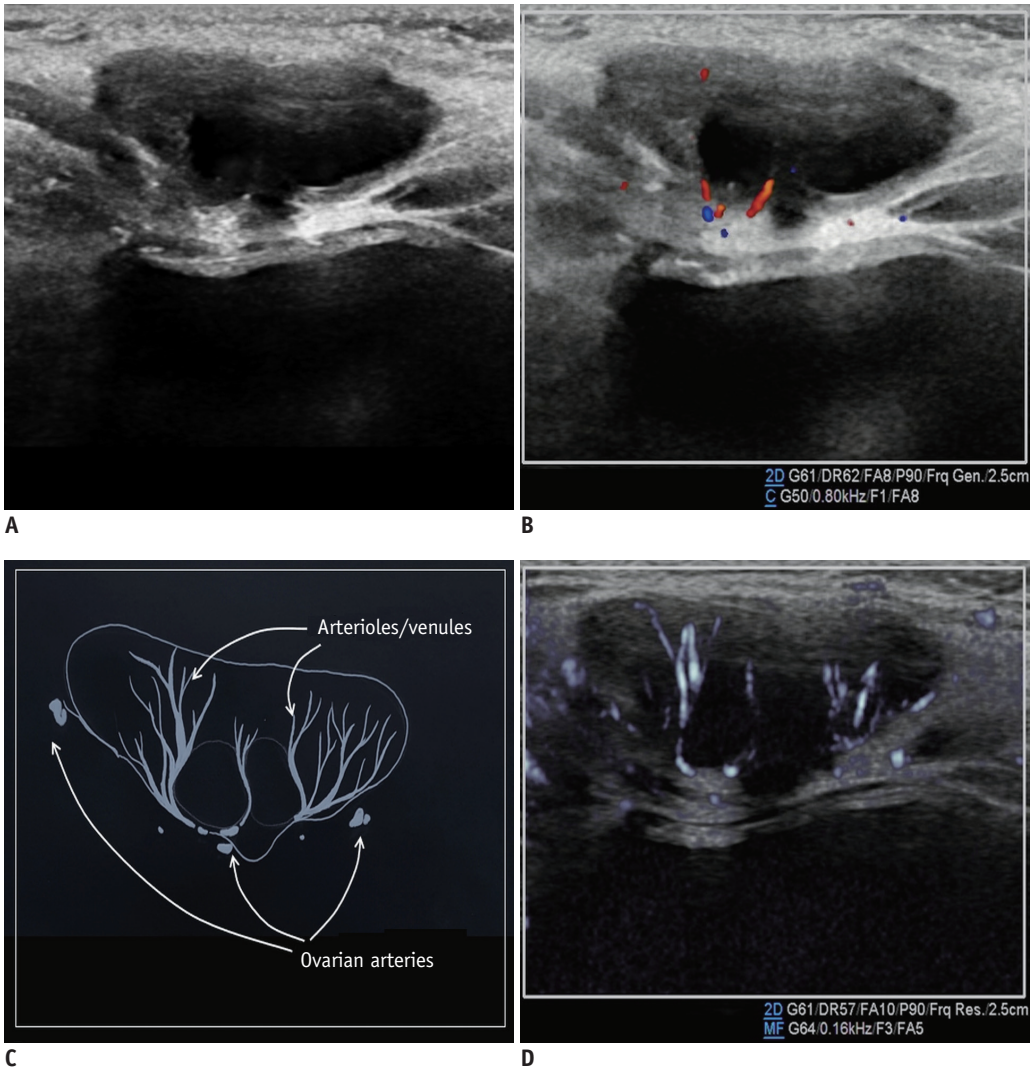

Fig. 10. Ovarian ultrasonography in 30-month-old girl with incarcerated left ovarian hernia.
A. Grayscale ultrasonography. **B.** Color Doppler ultrasonography shows ovarian arteries and veins close to hilum. **D.** Microvascular ultrasonography shows more arterioles traversing ovarian medulla to cortex, which are indicated on illustration **(C)**.

https://doi.org/10.3348/kjr.2019.0500

Korean Journal of Radiology
KJR

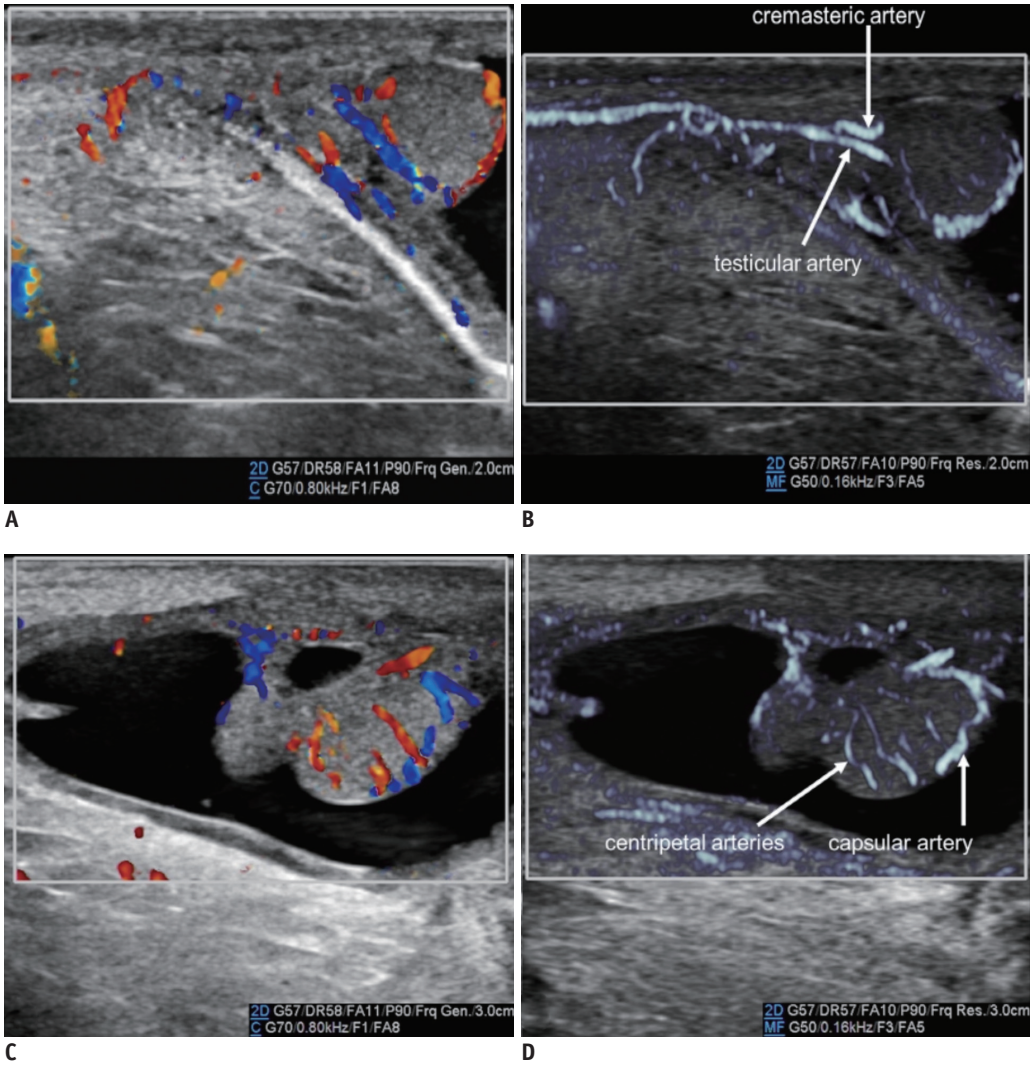

Fig. 11. Testicular ultrasonography longitudinal scan in 25-day-old boy with scrotal hydrocele.
Microvascular ultrasonography images **(B, D)** show testicular, cremasteric, capsular, and centripetal arteries better compared to color Doppler ultrasonography images **(A, C)**.

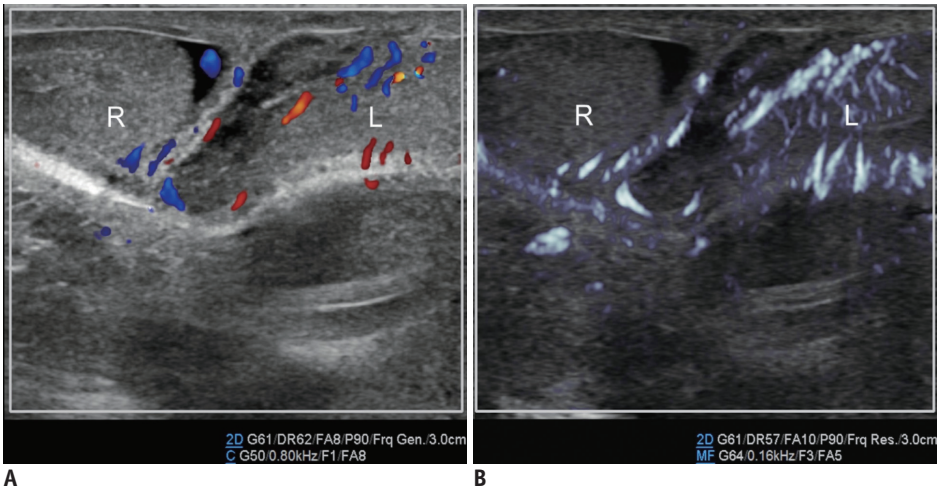

Fig. 12. Testicular ultrasonography transverse scan in 2-month-old boy with right inguinal hernia.
Perfusion of right testis (R) is lesser than that of left testis (L) because vascular pedicle is compressed by right inguinal hernia (not shown here). Perfusion differences between testes are more pronounced on microvascular ultrasonography **(B)** than on color Doppler ultrasonography **(A)**.

https://doi.org/10.3348/kjr.2019.0500

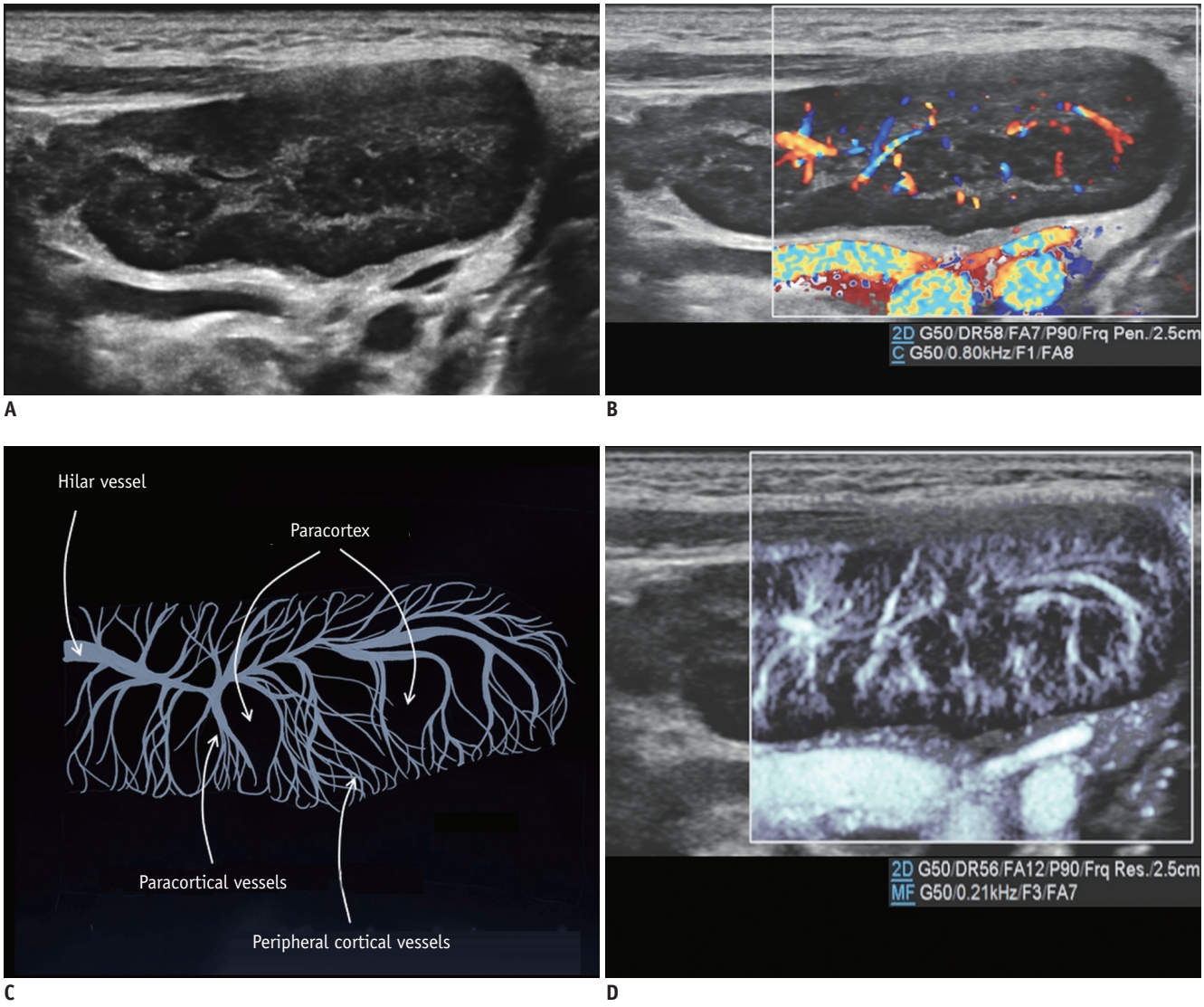

A B C D

Fig. 13. Reactive cervical lymphadenopathy in 4-year-old boy.
A. Grayscale ultrasonography. **B.** Color Doppler ultrasonography shows hilar and paracortical vessels. **C.** Illustration indicates hilar, paracortical, and peripheral cortical vessels and paracortices, as seen on microvascular ultrasonography **(D)**.

tool, which was the measured amount of blood flow in the defined region of interest, the features in our study were consistent with the features in a study by Bayramoglu et al. (12). They performed quantitative assessments using SMI for the thyroid glands, based on a vascularity index parameter that was significantly higher in patients with Hashimoto thyroiditis than in the controls (13.5% vs. 7.5%, respectively).

Kidney

The renal arteries enter the kidneys via the hila and have a primary bifurcation, which subsequently splits into the interlobar, arcuate, and interlobular arteries. The smaller branches comprise the glomerular and peritubular capillaries (13). MVUS demarcated the blood vessels in the renal cortex in children, and detailed branching of the interlobar, arcuate, and interlobular arteries supplying the renal cortex was demonstrated better on MVUS than on CDUS (Fig. 5). In addition, the renal medulla was clearly defined on MVUS as an oval, hypoechoic area. The superiority of MVUS compared to CDUS for depicting the interlobular arteries of the kidneys was illustrated when infection spread to the kidneys, and acute pyelonephritis (APN) developed. The pathophysiological changes in APN are characterized by interstitial edema, tubular obstruction, and vasoconstriction (14), and the correlated US findings are renal enlargement with changes in the parenchymal

https://doi.org/10.3348/kjr.2019.0500

Korean Journal of Radiology
KJR

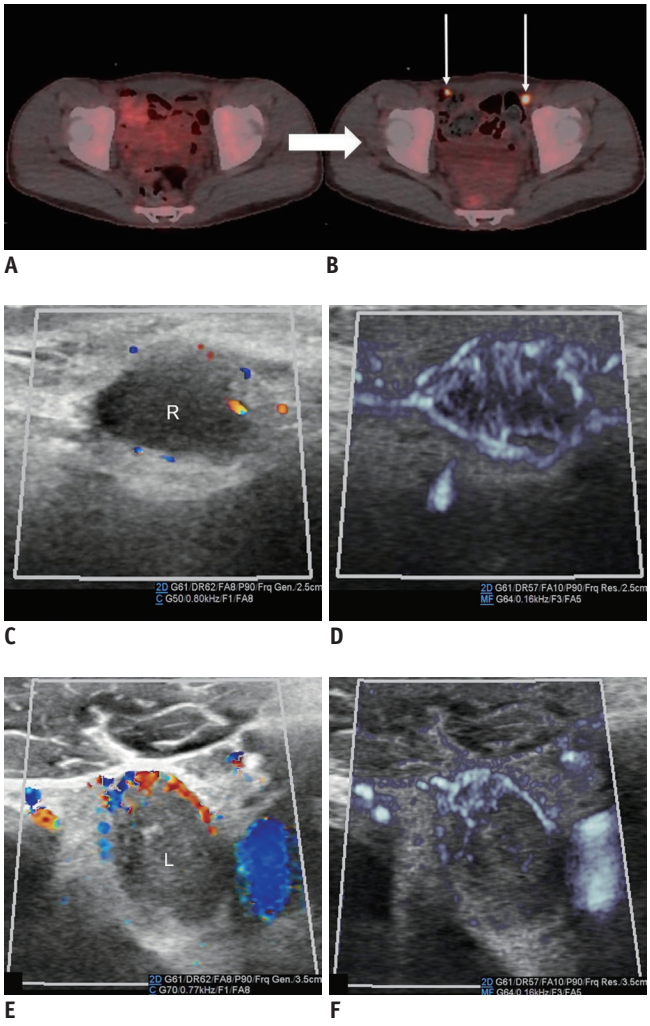

Fig. 14. Inguinal metastatic lymphadenopathies in 15-year-old boy with desmoplastic small round-cell tumor.
A, B. ^{18}F-F-FDG positron emission tomography/CT scans performed at 2-month intervals. Increased ^{18}F-F-FDG uptake (arrows) in bilateral inguinal lymph nodes on follow-up CT **(B)** suggests metastases. **C, D.** Right inguinal lymphadenopathy. **E, F.** Left inguinal lymphadenopathy. Microvascular ultrasonography **(D, F)** defines increased vascular structures better compared to color Doppler ultrasonography **(C, E)**. CT = computed tomography, ^{18}F-F-FDG = ^{18}F-fluorodeoxyglucose

echogenicity, loss of corticomedullary differentiation, collecting system dilatation, and areas of hypoperfusion (15). MVUS demonstrated localized areas of hypoperfusion because the difference in perfusion between the normal renal cortex and the involved area was more apparent on MVUS than on CDUS (Fig. 6). In addition, some children with APN showed stretching of the interlobar vessels, which might be caused by interstitial edema.

Urinary Bladder

Kim et al. (5) reported that MVUS could identify reversed flow of urine in the distal ureter and a swirl appearance of urine movement in the distended renal pelvis in patients with high-grade vesicoureteral reflux (VUR). In addition, we could detect the reversed flow of urine in a patient with grade 2 VUR (Fig. 7). Although MVUS is not feasible for visualizing the reversed flow of urine in all patients with VUR, it is apparent that MVUS is a non-invasive and safe method, without radiation exposure, unlike voiding cystourethrography. With color MVUS, the flow direction was confirmed more certainly.

Small Bowel

The vasa recta arising from the mesenteric arteries branch-out in a tree-like appearance at the mesenteric border of the small bowel, and subsequently, some branches pass directly into the bowel wall while some branches circumscribe the bowel anteriorly and posteriorly to anastomose freely at the antimesenteric border (16). MVUS demonstrated the small vessels circumscribing the bowel wall and even the transmural vessels, particularly where inflammation or infection occurred (Figs. 8, 9).

Ovary

The smaller branches of the ovarian arterial arcade penetrate the ovarian hilum and medulla, showing coiling and branching. In the medulla, each branch traverses to the ovarian cortex in a spiral shape, giving off branches that divide into the arterioles perpendicular to the ovarian surface (17). MVUS was feasible for evaluating the small spiral arterioles in the ovarian medulla (Fig. 10). Ayaz et al. (4) recently reported that improved detection of ovarian vascularity using SMI might provide additional information, such as factors of menarche or age affecting ovarian perfusion.

Testis

The main blood supply to the testis is provided by the testicular arteries from the aorta. In the scrotum, the testicular artery runs along the posterior aspect of the testis and flows through the tunica albuginea, branching off into two sets of arteries: the capsular and transmediastinal arteries. The capsular artery splits into the centripetal arteries that go through the testicular parenchyma and flow toward the mediastinum. As they reach the mediastinum, the centripetal arteries turn into the recurrent rami that flow back in the opposite direction, supplying blood from

https://doi.org/10.3348/kjr.2019.0500

the mediastinum to the testis (18). MVUS demonstrated the testicular, capsular, and centripetal arteries (Fig. 11) and was useful for assessing the status of testicular perfusion (Fig. 12). Lee et al. (7) reported that SMI was more sensitive than PDUS for detection of parenchymal perfusion of the undescended testis in young children.

Lymph Nodes

The hilar artery of the lymph node branches into the

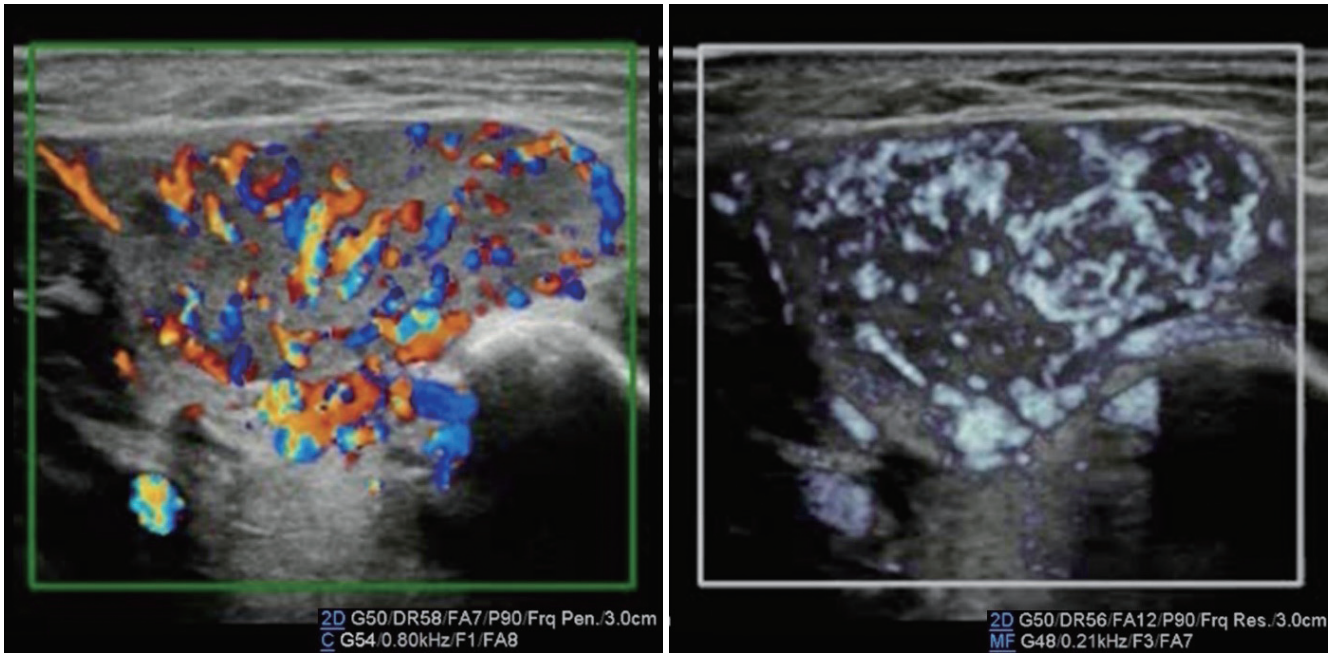

A B

Fig. 15. Infantile hemangioma of right parotid gland in 1-month-old boy.
Microvascular ultrasonography video clip (Supplementary Movie 4) **(B)** shows definition of margin and extent of mass better compared to color Doppler ultrasonography video clip (Supplementary Movie 3) **(A)**.

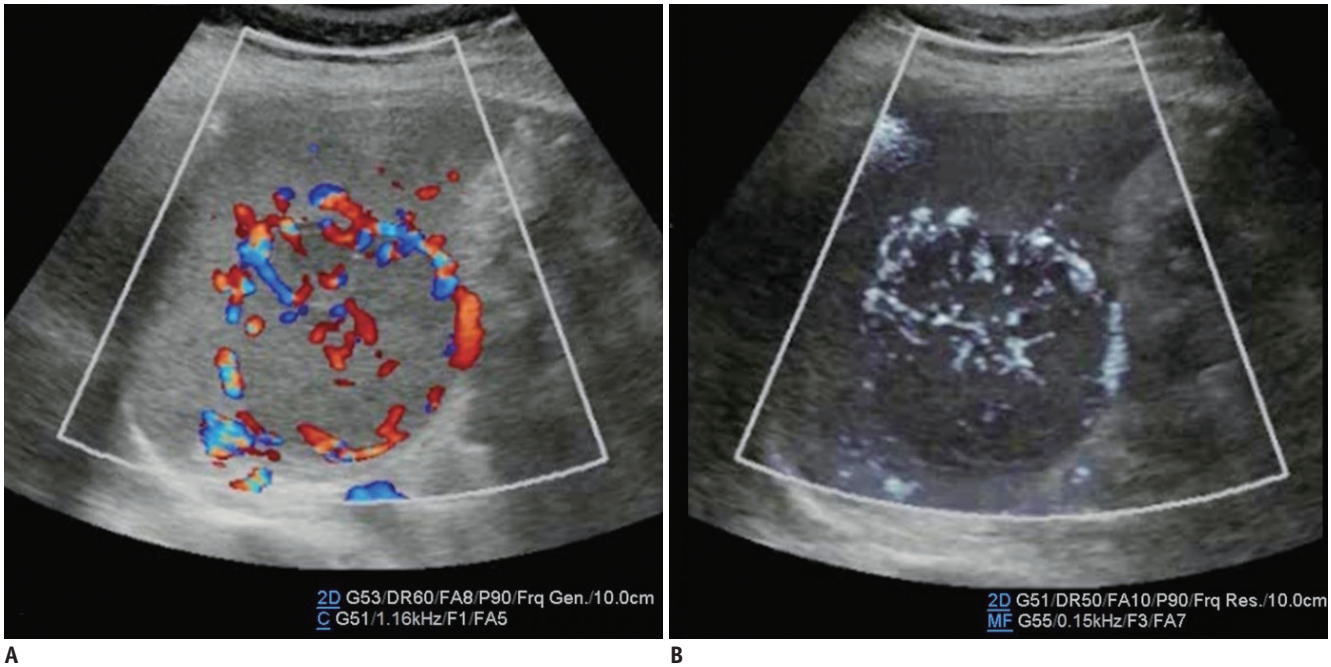

A B

Fig. 16. Cavernous hemangioma of spleen in 10-year-old boy.
Microvascular ultrasonography video clip (Supplementary Movie 6) **(B)** demonstrates small vessels within mass better compared to color Doppler ultrasonography video clip (Supplementary Movie 5) **(A)**.

https://doi.org/10.3348/kjr.2019.0500

Korean Journal of Radiology
KJR

medullary arterioles that radiate centrifugally and form a dense network of capillaries (19). Subsequently, the capillaries empty into the high endothelial venules, which transit to the medullary venules, returning centripetally to the hilar vein. CDUS showed the hilar vessels and medullary cords at the level of the central hilum and occasionally a deep cortical unit. In addition, MVUS allowed visualization of the paracortical vessels and even the peripheral cortical vessels that were not seen on CDUS (Fig. 13).

Metastatic lymphadenopathy tended to have peripheral vascularity, associated with tumor angiogenesis and the desmoplastic reaction or recruitment of the capsular vessels (20). Demonstration of increased peripheral vascular structures surrounding the lymph nodes by MVUS was better compared to that by CDUS (Fig. 14).

Vascular Lesions

Infantile hemangiomas are the most common tumors in children, and US is the preferred diagnostic imaging modality (21). Most cases of hemangioma manifest as cutaneous lesions in the head and neck (22), and we used MVUS for an infantile hemangioma that occurred in the parotid gland. US findings of the infantile hemangioma of the parotid gland included a well-circumscribed hypervascular mass with fast flow, confirmed using Doppler spectral waves (23). In our experience, CDUS was sufficient to diagnose infantile hemangiomas, but MVUS had the advantage of defining the margin and extent (Fig. 15).

Cavernous hemangioma of the spleen is a heterogeneously hypoechoic mass, and abundant blood flow may be detected on CDUS (24). In our experience, peripheral blood flow was well-depicted on CDUS, but the internal vascular network was visible in finer detail on MVUS (Fig. 16).

Advantages and Disadvantages of MVUS in Children

In our cases, MVUS demonstrated the microvascular structures and provided details of microvascular branching that were eliminated as clutter artifacts on CDUS. Therefore, MVUS detected the presence or absence of blood flow quickly to assess diseases in which changes in blood or urine flow occurred. MVUS and CDUS had the same technique, which included pressing a button to activate the function, and it was convenient and more comfortable than invasive examinations, such as contrast-enhanced US or voiding cystourethrography.

As with PDUS, MVUS was sensitive to motion and flash artifacts, which was considered a major drawback of the use of MVUS in young children. However, with advancements in the technology, the acquisition time has shortened. In addition, the maximal size of the region of interest activated on MVUS was smaller than that on CDUS.

CONCLUSION

We reviewed normal and abnormal perfusion patterns using MVUS for various tissues, including the brain, thyroid gland, kidney, urinary bladder, small bowel, ovary, testis, lymph node, and hemangiomas in children. Further clinical studies investigating the correlations between MVUS, pathologies, and clinical prognoses can extend the use of MVUS, and the quantification analysis can also enhance the diagnostic confidence of MVUS in children.

Supplementary Materials

The Data Supplement is available with this article at https://doi.org/10.3348/kjr.2019.0500.

Supplementary Movie Legends

Movie 1 shows normal urine flow from distal ureter to urinary bladder. **Movie 2** shows reversed urine flow from ureterovesical junction to distal ureter. **Movie 3** shows definition of margins and extent of infantile hemangioma of parotid gland better compared to **Movie 4**. **Movie 5** demonstrates small vessels within cavernous hemangioma of spleen better compared to **Movie 6**.

Conflicts of Interest

The authors have no potential conflicts of interest to disclose.

ORCID iDs

Bo-Kyung Je
https://orcid.org/0000-0001-8335-9980
Joonghyun Yoo
https://orcid.org/0000-0002-0394-7414
Ji Yung Choo
https://orcid.org/0000-0003-1244-0102

REFERENCES

1. Babcock DS, Patriquin H, LaFortune M, Dauzat M. Power doppler sonography: basic principles and clinical applications in children. *Pediatr Radiol* 1996;26:109-115
2. Park AY, Seo BK. Up-to-date Doppler techniques for breast tumor vascularity: superb microvascular imaging and contrast-enhanced ultrasound. *Ultrasonography* 2018;37:98-106
3. Goeral K, Hojreh A, Kasprian G, Klebermass-Schrehof K, Weber M, Mitter C, et al. Microvessel ultrasound of neonatal brain parenchyma: feasibility, reproducibility, and normal imaging features by superb microvascular imaging (SMI). *Eur Radiol* 2019;29:2127-2136
4. Ayaz E, Aslan A, İnan İ, Yıkılmaz A. Evaluation of ovarian vascularity in children by using the "superb microvascular imaging" ultrasound technique in comparison with conventional Doppler ultrasound techniques. *J Ultrasound Med* 2019;38:2751-2760
5. Kim HK, O'Hara S, Je BK, Kraus SJ, Horn P. Feasibility of superb microvascular imaging to detect high-grade vesicoureteral reflux in children with urinary tract infection. *Eur Radiol* 2018;28:66-73
6. Ohno Y, Fujimoto T, Shibata Y. A new era in diagnostic ultrasound, superb microvascular imaging: preliminary results in pediatric hepato-gastrointestinal disorders. *Eur J Pediatr Surg* 2017;27:20-25
7. Lee YS, Kim MJ, Han SW, Lee HS, Im YJ, Shin HJ, et al. Superb microvascular imaging for the detection of parenchymal perfusion in normal and undescended testes in young children. *Eur J Radiol* 2016;85:649-656
8. Duvernoy HM. *The human brain: surface, three-dimensional sectional anatomy with MRI, and blood supply*, 2nd ed. Wien: Springer-Verlag, 1999:429-458
9. Jiang ZZ, Huang YH, Shen HL, Liu XT. Clinical applications of superb microvascular imaging in the liver, breast, thyroid, skeletal muscle, and carotid plaques. *J Ultrasound Med* 2019;38:2811-2820
10. Machado P, Segal S, Lyshchik A, Forsberg F. A novel microvascular flow technique: initial results in thyroids. *Ultrasound Q* 2016;32:67-74
11. Chen L, Zhan J, Diao XH, Liu YC, Shi YX, Chen Y, et al. Additional value of superb microvascular imaging for thyroid nodule classification with the thyroid imaging reporting and data system. *Ultrasound Med Biol* 2019;45:2040-2048
12. Bayramoglu Z, Kandemirli SG, Caliskan E, Yilmaz R, Kardelen AD, Poyrazoglu S, et al. Assessment of paediatric Hashimoto's thyroiditis using superb microvascular imaging. *Clin Radiol* 2018;73:1059.e9-1059.e15
13. Chade AR. Renal vascular structure and rarefaction. *Compr Physiol* 2013;3:817-831
14. Kim B, Lim HK, Choi MH, Woo JY, Ryu J, Kim S, et al. Detection of parenchymal abnormalities in acute pyelonephritis by pulse inversion harmonic imaging with or without microbubble ultrasonographic contrast agent: correlation with computed tomography. *J Ultrasound Med* 2001;20:5-14
15. Craig WD, Wagner BJ, Travis MD. Pyelonephritis: radiologic-pathologic review. *Radiographics* 2008;28:255-277
16. Eisberg HB. Intestinal arteries. *Anat Rec* 1924;28:227-242
17. Clement PB. Histology of the ovary. *Am J Surg Pathol* 1987;11:277-303
18. Lotti F, Maggi M. Ultrasound of the male genital tract in relation to male reproductive health. *Hum Reprod Update* 2015;21:56-83
19. Willard-Mack CL. Normal structure, function, and histology of lymph nodes. *Toxicol Pathol* 2006;34:409-424
20. Ahuja A, Ying M. Sonography of neck lymph nodes. Part II: abnormal lymph nodes. *Clin Radiol* 2003;58:359-366
21. Darrow DH, Greene AK, Mancini AJ, Nopper AJ; Section on Dermatology, Section on Otolaryngology-Head and Neck Surgery, And Section on Plastic Surgery. Diagnosis and management of infantile hemangioma: executive summary. *Pediatrics* 2015;136:786-791
22. Fishman SJ, Mulliken JB. Hemangiomas and vascular malformations of infancy and childhood. *Pediatr Clin North Am* 1993;40:1177-1200
23. Weber FC, Greene AK, Adams DM, Liang MG, Alomari MH, Voss SD, et al. Role of imaging in the diagnosis of parotid infantile hemangiomas. *Int J Pediatr Otorhinolaryngol* 2017;102:61-66
24. Vancauwenberghe T, Snoeckx A, Vanbeckevoort D, Dymarkowski S, Vanhoenacker FM. Imaging of the spleen: what the clinician needs to know. *Singapore Med J* 2015;56:133-144

https://doi.org/10.3348/kjr.2019.0500